



FRACTAL: An Ultra-Large-Scale Aerial Lidar Dataset for 3D Semantic Segmentation of Diverse Landscapes

Charles Gaydon

Michel Daab

Floryne Roche

Institut national de l'information géographique et forestière (IGN), France

fractal.dataset@ign.fr

Abstract—Mapping agencies are increasingly adopting Aerial Lidar Scanning (ALS) as a new tool to monitor territory and support public policies. Processing ALS data at scale requires efficient point classification methods that perform well over highly diverse territories. To evaluate them, researchers need large annotated Lidar datasets, however, current Lidar benchmark datasets have restricted scope and often cover a single urban area. To bridge this data gap, we present the FRENCH ALS Clouds from TArgeted Landscapes (FRACTAL) dataset: an ultra-large-scale aerial Lidar dataset made of 100,000 dense point clouds with high quality labels for 7 semantic classes and spanning 250 km². FRACTAL is built upon France's nationwide open Lidar data. It achieves spatial and semantic diversity via a sampling scheme that explicitly concentrates rare classes and challenging landscapes from five French regions. It should support the development of 3D deep learning approaches for large-scale land monitoring. We describe the nature of the source data, the sampling workflow, the content of the resulting dataset, and provide an initial evaluation of segmentation performance using a performant 3D neural architecture.

Key Figures

- 250 km² of data sampled from 17,440 km² in 5 French regions
- 100,000 point clouds - 50 x 50 m each
- 9261M points from high density ALS (37 pts/m²)
- 7 semantic classes: other, ground, vegetation, building, water, bridge, permanent structure

I. INTRODUCTION

A. Aerial Lidar Scanning for land monitoring

High-density ALS is now recognized as a powerful remote sensing modality to support important public actions such as ecological monitoring [1] and risk management (floods [2], forest fires [3]). Detailed 3D mapping also contribute to the consolidation of existing geographic databases. The reduction in costs associated with the acquisition, storage, processing, and dissemination of Aerial Lidar Scanning (ALS) data has paved the way for its production at unprecedented scales. In recent years, ALS has been increasingly used by public authorities at the regional and national levels. In a comprehensive report, [4] describe the availability of non-commercial Lidar data across Europe: at least a dozen European countries have already made

nationwide Lidar acquisitions, with densities of 10 to 40 pts/m². In France, the national mapping agency (Institut national de l'information géographique et forestière, IGN) aims to map the entire French territory with high-density ALS point clouds (10 pulses/m², about 40 pts/m²) by 2026, in a program called Lidar HD (for "High Density") [5].

B. Challenges and methods for point cloud classification

Point cloud classification is a prerequisite to any downstream use of Lidar products. Ground points must be identified to produce accurate Digital Terrain Models (DTMs) and separated from vegetation points to normalize tree heights in forest applications, e.g. for forest biomass estimation. Buildings are reconstructed from building points for urban modeling, while city trees are mapped from clusters of vegetation points to manage urban biodiversity.

Understanding Lidar data requires specialized knowledge and tools. Many softwares exist for Lidar feature extraction (e.g. TopoDOT [6], TerraScan [7]...), however, each has its own strengths and weaknesses, and they all require some form of manual input to reach satisfying results [8]. The complexity, volume, and lack of structure of Lidar data make manual labelling time and labor-intensive. There is therefore a critical need for more automated methods.

Recently, there has been a surge in the development of deep learning approaches for the efficient semantic segmentation of point clouds. PointNet in 2016 [9] and PointNet++ in 2017 [10] paved the way by proposing a framework to process unordered point clouds without costly preprocessing. We refer the reader to Section 4 of a previous work [11] for a short history of the development of 3D deep learning architectures.

C. The need for diversity in ALS benchmark datasets

ALS differs from ground-based Lidar in critical ways: airborne Lidar has nadir orientation instead of lateral orientation, and a lower but more homogeneous point density [12]. Most importantly, airborne Lidar can be used to collect data at a much larger scale than ground-based Lidar, which adds specific challenges to their classification. Vast territories the size of a country have diverse landscapes and vegetation, along with unique signs of human activity, leading to high intraclass heterogeneity. Additionally, geographic data are characterized by spatial autocorrelation, and a long-tail distribution, resulting in a

TABLE I: Benchmark datasets for 3D semantic segmentation of ALS data. We include the datasets listed by [13] along with their proposed benchmark dataset CENAGIS-ALS, and our own dataset FRACTAL. ALS: Aerial Lidar Scanning; ULS: Unmanned Lidar Scanning.

Reference	Year	Sensor Platform	Area (km ²)	Classes	Points	Density (pts/m ²)
Vaihingen (ISPRS) [15]	2012	ALS	0.1	9	1.16M	4-7
DublinCity [16]	2015	ALS	2	$9 \in 7 \in 4$	260M	348
LASDU [17]	2020	ALS	1.02	5	3.12M	3-4
DALES [12]	2020	ALS	10	8	500M	50
Hessigheim 3D [18]	2021	ULS	0.19	11	74M	800
OpenGF [14]	2021	ALS	47.7	2	542M	11
CENAGIS-ALS [13]	2023	ALS	2	$49 \in 28 \in 7$	550M	275
FRACTAL (Ours)	2024	ALS	250	7	9261M	37

variety of rare scenes that may be spatially concentrated i.e. globally rare but locally frequent like wind turbines or greenhouses.

The specific nature and scope of ALS must be addressed in the evaluation of 3D point cloud semantic segmentation methods. In doing so, having large representative annotated datasets is critical, however, current benchmark datasets come up short: they are limited in size and spatial diversity, typically covering a single area, and thus cannot attest to the capacity of 3D deep learning models to deal with the challenges of large-scale land monitoring.

[13] make a comprehensive review of current Lidar benchmark datasets for 3D point cloud semantic segmentation as of October 2023. They list 26 datasets of which only 6 have ALS data, which we report in Table I. To date, OpenGF [14] is the largest of them: it spans almost 50 km² and explicitly includes diverse landscapes. Interestingly, OpenGF is built from open large-scale ALS archives from 4 countries in 3 continents, via a careful selection of areas with high-quality point annotations in diverse landscapes (i.e. metropolis, small city, village, mountain). Authors demonstrate the effectiveness of leveraging open Lidar assets to quickly create high-quality, diverse, large-scale benchmark datasets for 3D semantic classification.

OpenGF is, however, tailored for the specific task of ground/non-ground classification and was stripped of the semantic classes used in most applications (e.g., building, vegetation...). The other ALS benchmark datasets only span a single urban area, and we observe that rich semantics and high point densities are only made available in small volumes. The Dayton Annotated Lidar Earth Scan (DALES) [12] attempts to offer the level of detail required for typical urban applications, with 8 semantic classes and a high point density of 50 pts/m². Covering an area of 10 km², DALES is the largest dataset of its kind. However, with a single urban area, it falls far short of the landscape diversity found in EO applications.

D. Contributions

This data gap motivates us to release the French ALS Clouds from Targeted Landscapes, or FRACTAL. FRACTAL is a large dataset for the semantic segmentation

of ALS data that spans 250 km². FRACTAL is made of 100,000 distinct point clouds, each spanning 50 × 50 m and typically containing 20k to 40k labelled points (37 pts/m² on average).

The dataset is built from the French Lidar HD data [5], using a sampling scheme that explicitly concentrates rare classes, rare objects, and challenging landscapes. Being sampled from an initial area of 17,440 km² in 5 French regions, it is characterized by a high diversity of scenes.

Point clouds are labelled with seven common semantic classes: ground, vegetation, building, water, bridge, permanent structure, and other. The labels were produced with automated processes and then verified and corrected by Lidar operators to achieve high quality classification. FRACTAL is overall the largest open benchmark dataset for 3D semantic segmentation, and the first to offer the diversity of landscapes inherent to large-scale land monitoring. It provides a challenging benchmark dedicated to the development of 3D deep learning methods.

We make the following contributions:

- Define a general framework to catalog and sample diverse point clouds from large open ALS archives.
- Introduce FRACTAL: a benchmark dataset for 3D point cloud semantic segmentation, sampled from verified areas of the French Lidar HD data. The sampling has explicit consideration for spatial diversity and landscape diversity, making FRACTAL suitable for the evaluation of point cloud classification methods against the specific challenges of land monitoring.
- Set a baseline evaluation of segmentation performance on the dataset using a state-of-the-art deep learning method to show its potential for benchmarking.

Section II presents the data sources used to create FRACTAL. Section III describes the strategy used for cataloguing and sampling data patches at scale into a deep learning benchmark dataset. Section IV presents the resulting dataset itself.

II. DATA SOURCES

We achieve efficient, large scale dataset creation by leveraging an open ALS data archive: the Lidar HD data. To reflect real-world Lidar processing practices, clouds are

colorized from national Very High Resolution (VHR) aerial imagery from the ORTHO HR database.

A. ALS point clouds

The Lidar HD program [5] is a national initiative that aims to provide a 3D description of the French territory by 2026, using high-density ALS (10 pulses/m² or about 40 pts/m²). Designed to meet the needs of public actions (flood prevention, estimation of forest resources, etc.), it is operated by the IGN with both internal resources and subcontracted assistance. The data acquired and produced as part of this program (i.e., point clouds, Digital Terrain Models, Digital Surface Models) are made available as open data with extensive documentation [19].

The program covers mainland France and its overseas territories for a total of 550,000 km². The program consists of four phases: data acquisition, storing, processing, and dissemination, along user support. The data acquisition and processing are sequenced in blocks of 50 x 50 km and must be compatible with a variety of Lidar sensors (Leica, Riegl, and Teledyne/Optech), acquisition seasons (leaf-on or leaf-off), and landscapes (urban, rural, mountains, seashores, overseas territories, etc.).

Processing includes the semantic segmentation of point clouds into 11 classes: unclassified, ground, vegetation (low, medium, and high), buildings, water, bridge deck, permanent structures, artefact, synthetic. We detail the specification of this nomenclature in Appendix A.

In addition, the classification of Lidar HD data may come in one of two flavors:

Classified Lidar HD: results from a fully automated classification process operated by the IGN, consisting of explicit detection methods using the IGN’s national databases and the results of AI deep learning models.

Optimized Lidar HD: results from automatic classification processing followed with manual corrections by subcontractors. The classification is audited by the IGN via a visual inspection of 10% of the delivered point clouds. In the audit, all classification errors are listed and rated for severity, with particular attention to confusions in buildings, bridges and ground. Consolidated error scores are computed, first for each of these three critical semantic classes, then globally. These scores are required to be under specific thresholds for the classification to be validated. Particular attention is given to the exhaustivity of individual buildings, with a target recall of 99.9% in high-stakes areas (e.g. flood-prone, urban...) and a target recall of 99.5% elsewhere.

B. VHR aerial images

The ORTHO HR® [20] is a mosaic of VHR aerial images acquired during national surveys. Every year, about a third of French metropolitan territory is updated. The individual images are mapped onto a cartographic coordinate reference system and projected on the RGE ALTI Digital Terrain Model for orthorectification. ORTHO HR images have a high spatial resolution of 0.20 m, and near infrared,

red, green and blue channels. Radiometric processing methods, including equalization and global correction, are applied to obtain the final product. The radiometry of the red, green, and blue channels cannot be considered a physical measurement of channel reflectance due to variations in acquisition dates and specific radiometric corrections applied for visual appealing.

Aerial surveys are not synchronized with Lidar HD acquisitions and a variable time lag of up to 3 years might separate them. This is because aerial images from the ORTHO HR are renewed every three years, while Lidar data are processed as soon as they are acquired. In the interim, buildings may have been constructed and vegetation may have expanded or been cleared. Moving elements such as vehicles are unlikely to be consistent. Also, the appearance of cultivated fields is likely to be inconsistent between modalities due to different seasons of acquisition.

III. SAMPLING METHODOLOGY

A. Sampling area

At the time of dataset creation, Lidar HD data is available for about half of metropolitan France, mainly in its southern half. To have the highest possible annotation quality, we restrict our sampling to Optimized Lidar HD i.e., to the areas that went through human verification and audit of the classification. Figure 1 presents the 5 spatial domains we consider, each spanning 3456 km² on average, and distant from at least 100 km from one another. The spatial domains compose a sampling area of 17,440 km² in Southern France.

To define a common setting for the benchmark of deep learning models, we reserve an area for testing in each spatial domain. Each of the 5 test areas span 210 km² on average, for a total test sampling area of 1049 km². Having only a limited number of spatial domains with their own unique characteristics (seashores, mountains, field crops, etc.), test data and train data share the same spatial domains. Test areas are however contiguous, large, and distinct from the train areas. This enables spatial block validation and reduces the influence of spatial autocorrelation on model evaluation, which is critical when evaluating remote sensing solutions [21].

B. Dataset size and sample unit

We aim to produce a manageable dataset with suitable size for common research practices and computing infrastructures. Based on our own experience with training semantic segmentation models on Lidar HD data, we set a target dataset size of 250 km² - a 70-fold reduction compared to the initial sampling area.

The sample unit is a 50 × 50 m square patch. We have found that such a width provides a good balance between detailed structures and long-range dependencies. A square shape facilitates data extraction and visualization of data patches. Also, training models on square point clouds favors

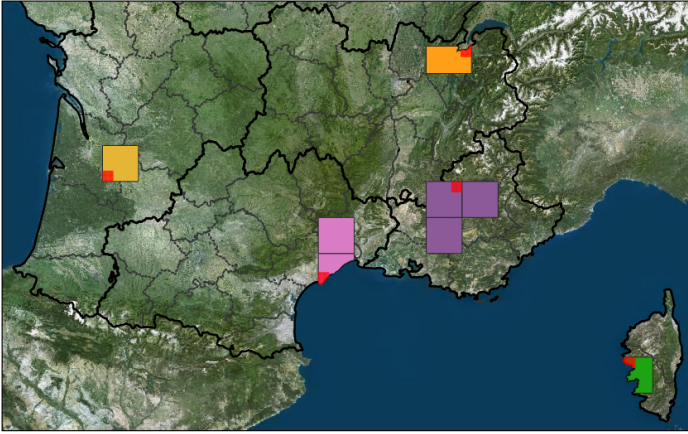


Fig. 1: The five spatial domains composing the 17,440 km² of the sampling area. The 1,049 km² of area reserved to sample the test set are highlighted in red.

the use of non-overlapping tiling at inference time, thus gaining efficiency by limiting redundant predictions.

C. Considerations for dataset diversity

We adopt the following design principles to sample the dataset:

Class rebalancing: We explicitly address class imbalance, which is often detrimental to model training, by up-sampling rarer classes such as water, bridge, and permanent structure.

Uncertainty sampling: We aim to increase the representation of scenes known to be challenging for classification models by upsampling specific landscapes and hardscapes, such as mountainous areas, seashores, or complex urban scenes.

Spatial sampling as a proxy for scene diversity: Given the spatial autocorrelation of geographic data, we aim for the broadest spatial distribution of samples. This maximizes diversity within each category of scenes and globally.

D. Cataloguing of available data

For efficient consideration of classes and landscapes, we need a detailed representation of all available data of the sampling area with patch resolution. This representation takes the form of a geographical database called the Lidar Patch Catalog (LiPaC).

Cataloging data boils down to two steps, listing and describing, which we illustrate in Figure 2. We start by regularly dividing the sampling area into 50×50 m patches. We then describe all patches with two sets of descriptors: Lidar descriptors and vector descriptors. Lidar descriptors are derived from the Lidar data patches themselves: number of points in each semantic class, elevation (above sea level), and elevation gain. Vector descriptors are derived by spatial crossing with the BD TOPO® [22], a 3D vector description of the French territory and its infrastructures (buildings, roads, etc.). In the LiPaC, we include information about the following classes of objects: greenhouses, antennas, pylons,

highways, parking lots, water surfaces, greenhouses, pylons, antennas, and industrial, commercial, or agricultural buildings.

The LiPaC is a comprehensive tool for flexible and efficient sampling of all Lidar tiles under consideration. Its implementation as a PostGIS database gives us the full power of SQL syntax to select data and further characterize each Lidar patch with bespoke SQL queries that combine simple descriptors into more complex ones. We define two categories of high-level Boolean flags, which we report in Figure II. The first category contains 12 scene flags related to the semantic classification of the point cloud and the presence of certain objects within a semantic class. For example, we define a BUILD flag for patches that contain some points classified as buildings ($n \geq 500$ pts) and a BUILD_GREENHOUSE flag for patches that intersect greenhouses. The second category contains 7 scene flags that characterize patches in terms of landscapes, using heuristic definitions. For example, a patch is flagged as SEASHORE if it contains water ($n \geq 50$ pts) and ground ($n \geq 100$ pts) and is within 10 m of sea level.

E. Patch sampling

Having a detailed description of each patch makes it easy to rebalance semantic classes and ensure that challenging or rarer types of scenes are represented in the dataset, following the design principles established in Section III-C. We adopt a simple but effective sampling scheme consisting of targeted sampling followed by completion sampling:

Targeted sampling: For each scene type (i.e., flag), we perform spatially stratified sampling, i.e., we sample patches with stratification on 1×1 km Lidar HD tiles until a minimum concentration of that scene type is reached. Each sampling is performed independently, with replacement, to ensure that the spatial diversity within each group is optimal. As a result, the final proportion of each scene type may be higher than the minimum requirement. We set a target requirement for each scene type so that approximately 50% of the final dataset is found using targeted sampling (see Table II).

Completion sampling: The rest of the dataset is found by spatially stratified sampling without considering the flags. This is to ensure that we include more ordinary scenes such as field crops and rural areas, which are the majority.

F. Dataset split

We define a reference split into train, val, and test sets with an 80/10/10 ratio: 225 km² of data is used for model training, of which 25 km² is reserved for in-training evaluation, and 25 km² of data is sampled from test areas and kept for model evaluation. Train and test areas are sampled independently with the same sampling parameters.

Patches for in-training validation are sampled from the train areas with spatially stratified stratification, independently for each scene type. This results in the widest possible spatial distribution for each type of scene and ensures that all landscapes are equally represented

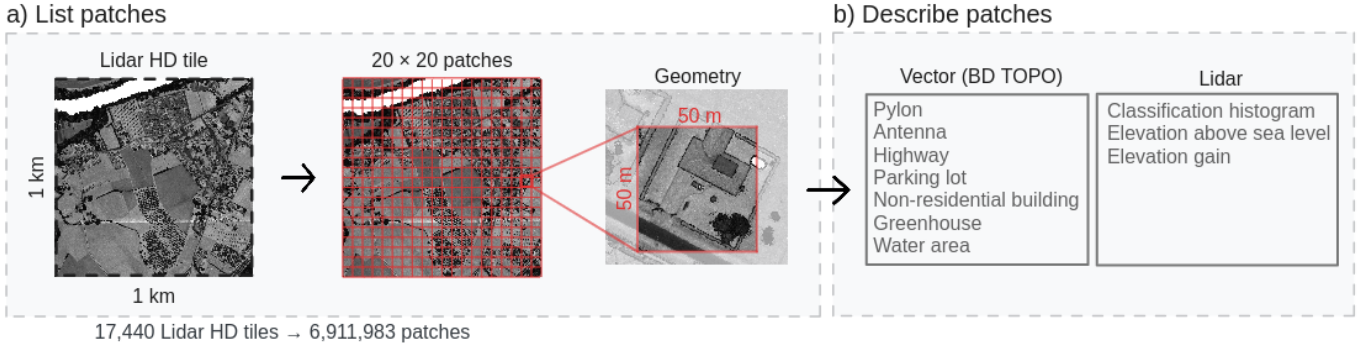


Fig. 2: Key steps involved in setting up a Lidar Patch Catalog (LiPaC) i.e. the geographical database that we use to a) list and b) describe all candidate Lidar patches for sampling.

TABLE II: Scene types and their target minimal concentration for targeted sampling.

Motivation	Scene Type	Definition	Target (%)	
Classes	BUILD	building ≥ 500 pts	8	
	BUILD_GREENHOUSE	greenhouse (BD TOPO)	1	10
	BUILD_BIG	non-residential building (BD TOPO)	1	
	BRIDGE	bridge ≥ 50 pts	5	5
	WATER	eau ≥ 50 pts	4	
	WATER_SURFACE	water area (BD TOPO) & eau ≥ 50 pts	1	5
	PERMSTRUCT	permanent structure ≥ 50 pts	3	
	PERMSTRUCT_PYLON	pylon (BD TOPO) & permanent structure ≥ 50 pts	1	5
	PERMSTRUCT_ANTENNA	antenna (BD TOPO) & permanent structure ≥ 50 pts	1	
	OTHER	unclassified ≥ 250 pts	3	
	OTHER_PARKING	parking lot (BD TOPO) & unclassified ≥ 250 pts	1	5
	OTHER_HIGHWAY	highway (BD TOPO) & unclassified ≥ 400 pts	1	
Landscapes	FOREST	high vegetation $\geq 90\%$ of points	5	
	HIGHSLOPE1	$35 \text{ m} \leq \text{elevation gain} < 45 \text{ m}$	2	
	HIGHSLOPE2	elevation gain $\geq 45 \text{ m}$	2	20
	MOUNTAIN	elevation $\geq 1000 \text{ m}$	4	
	WATER_ONLY	water ≥ 50 pts & ground = 0 pts	1	
	SEASHORE	$-10 \leq \text{elevation} < 10$ & water ≥ 50 & ground ≥ 100 pts	1	
	URBAN	building $\geq 25\%$ of points	5	

in the train and val sets. Refer to Appendix D for the proportions of scene types in each set.

G. Data extraction and colorization

From the sampled $50 \times 50 \text{ m}$ geometric patches, we extract the corresponding ALS point clouds. We colorize point clouds using near infrared, red, green and blue channels from the ORTHO HR images, based on the vertical alignment of points and pixels. Colorization is done regardless of potential obstructions: for instance, a ground point beneath a tree will be colored with the spectral information of the tree above it.

Point clouds are made available in the LAZ 1.4 format defined by the American Society for Photogrammetry and Remote Sensing (ASPRS) [23]. The following dimensions are particularly relevant for semantic segmentation: xyz

coordinates in Lambert 93 spatial reference system (EPSG:2154), intensity (16-bits encoding), return number and number of returns, scan angle, and near-infrared, red, green and blue (16-bits encoding). The Lidar HD classification nomenclature, described in Appendix A, is left intact in the data patches.

Except for its colorization, point clouds in FRACTAL inherit the characteristics of the Lidar HD data, and we refer users to Section 2.2 of their official product description [19] for more information.

IV. FRACTAL: THE DATASET

In this subsection, we present the resulting dataset, which we name FRACTAL: French ALS Clouds from Targeted Landscapes.

Section IV-A presents the characteristics of the dataset

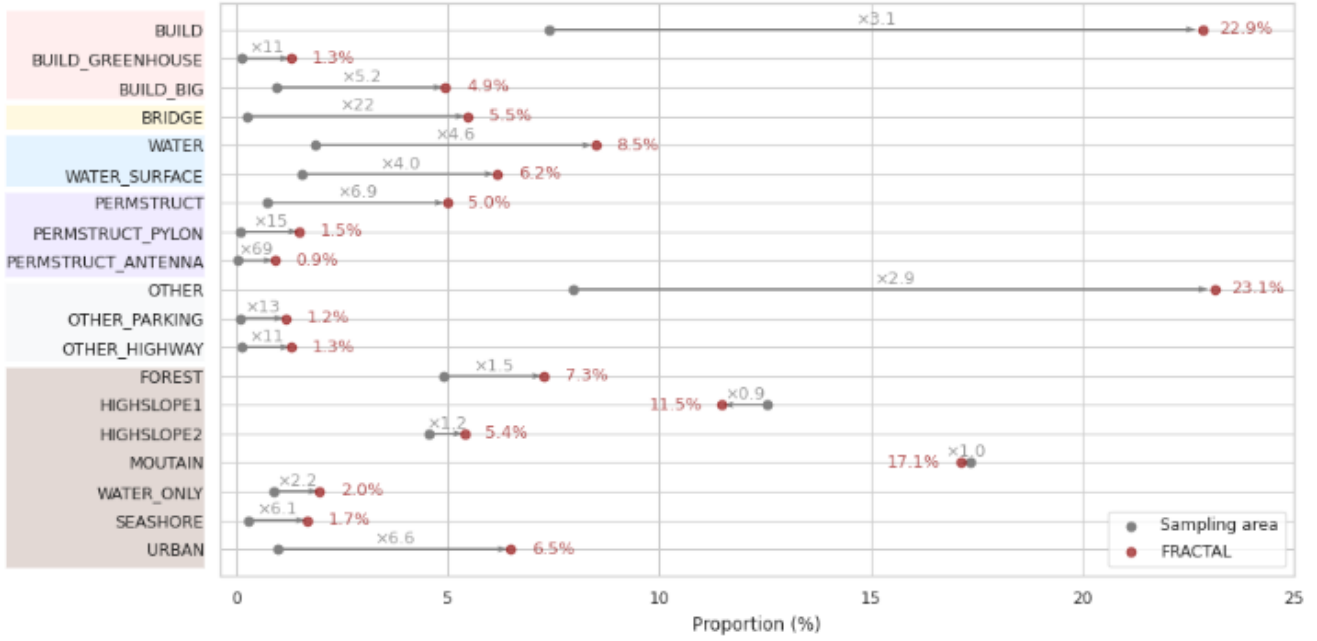


Fig. 3: Proportional gain of each scene type in FRCTAL after sampling.

itself and emphasizes its diversity. Section IV-B documents the file structure itself. Section IV-C list limitations to consider when using the dataset.

A. Spatial and semantic diversity

Table III presents key figures of the dataset, namely its size expressed in number of points, number of tiles, number of patches, and total area. We compare these figures with those of the sampling area to highlight that, while the dataset has been substantially reduced in size to facilitate manageable research, it still retains spatial diversity. Despite being 70 times smaller, the dataset incorporates data from all 17,440 initial tiles, ensuring comprehensive representation.

TABLE III: Size, areas, and number of points in FRCTAL compared to the sampling area. r = ratio.

	Sampling area	→	FRCTAL	r
Tiles	17440	→	17440	1
Area (km ²)	17440	→	250	70
Patches	6976000	→	100000	
Points (M)	661998	→	9261	71

Half of the dataset is found by targeted sampling of scene descriptors (47,253 patches, or 47.3%), the rest by completion sampling (52,747 patches, or 52.7%). The target minimum concentration is achieved for all descriptors except one: scenes with permanent structure points and with an antenna in the BD TOPO could not be concentrated to 1% in the train (target of $n = 1000$ patches) and test (target of $n = 100$ patches). Only 830 and 65 patches matching this description were found, respectively.

Figure 3 illustrates the proportional gain of each descriptor. The gain is most significant for rarer classes, with up to a 22-fold concentration of bridges. There is a reduction in the proportion of scenes with a slope in the $[35\text{ m}; 45\text{ m}]$ range: these are common scenes, concentrated in mountainous areas, which may therefore be undersampled by the full sampling.

Figure 5 shows the distribution of FRCTAL’s patches in a small area of 4×6 Lidar HD tiles. The 182 patches are highlighted in yellow (targeted sampling) and cyan (completion sampling). They are scattered and cover only 1.9% of the 24 km^2 (52-fold reduction). Validation patches are marked with a black cross and are homogeneously distributed across both Lidar HD tiles and scene types. Two Lidar HD tiles are framed in red, which we look at in more detail in Figure 6. We observe that the targeted sampling (in yellow) over-concentrates specific landscapes such as water surfaces, specific classes such as buildings, and specific human-made structures such as parking lots, industrial buildings, and electricity pylons. 5 patches were selected by completion sampling (in cyan). Among them, 4 do not contain any scene type flag. This illustrates the scarcity of more complex scenes in geographical data and the need to explicitly target them to obtain a challenging and diverse dataset.

B. File Structure

Figure 4 illustrates the dataset’s file structure. The point clouds are organized by set (train, val, and test), in 100 subdirectories of 1000 point clouds each. The naming convention for data patches is shown in the figure, where `tile_id` gives the X and Y kilometer northwest coordinates of the Lidar HD tile in the

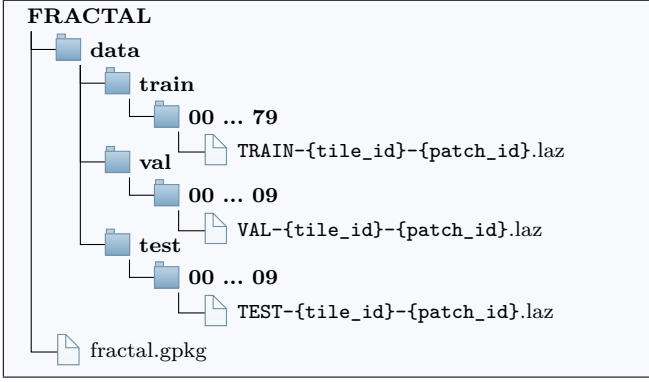


Fig. 4: Structure of files and directories in FRACTAL.

Lambert 93 projection (EPSG:2154), and `patch_id` is a unique, arbitrary patch identifier. For instance, patch `TEST-0744_6246-006804306.laz` belongs to the test set, was extracted from Lidar HD tile whose top left coordinates are $X = 0744$ and $Y = 6246$, and its unique identifier is 006804306.

The geometries of all patches and their descriptions are provided in a metadata file: `fractal.gpkg`.

C. Limitations and recommendations

FRACTAL is sampled from an existing open ALS archive, and shares its limitations. The dataset only includes data that underwent human corrections and auditing (i.e. “Optimized Lidar HD”), however, the specification of the Lidar HD classification includes a tolerance for errors. This tolerance is class specific: for instance, a perfect 100% recall for individual buildings is not mandatory as explained in Section II-A). Beyond actual errors, the very definition of “unclassified” points leads to potential confusions with other classes which we discuss in Section V-A. Considering the size of the dataset, these imperfections are expected to have a negligible impact for model evaluation, but users should be aware that they exist when inspecting the data.

Point clouds are colorized with asynchronous aerial imagery, which can lead to color artifacts (typically for moving objects such as vehicles) and misalignment between colors and shapes that can blur segmentation boundaries (e.g., roof points colored by a nearby tree). Mitigation strategies such as color augmentation and randomly dropping color dimensions may help reduce models’ reliance on color information.

Using FRACTAL to train models for production purposes should be done with caution. Indeed, the dataset covers 5 spatial domains from 5 southern regions of metropolitan France. While large and diverse, it only covers a fraction of the French territory and is not representative of its full diversity regarding either landscapes or human-made structures. Furthermore, domain shifts are frequent for aerial images due to different acquisition conditions and downstream data processing. When using models trained on the dataset to predict a classification in unseen regions, one should make the adequate verification and not

TABLE IV: Relation between the Lidar HD classification nomenclature and its adaptation in FRACTAL.

Lidar HD	→	FRACTAL
Unclassified	→	Other
Ground	→	Ground
Low vegetation		
Medium vegetation	→	Vegetation
High vegetation		
Buildings	→	Building
Water	→	Water
Bridge deck	→	Bridge
Permanent structures	→	Permanent structure
Artefact		-
Synthetic		-

assume its capacity to generalize. Similarly, considering new Lidar sensors should be done carefully. ALS data of comparable point densities (about 40 pts/m²) are expected to have consistent geometric characteristics, but users should still assess the model’s accuracy when predicting from alternative 3D data sources.

V. BASELINE EVALUATION

A. Task and metrics

FRACTAL is a benchmark dataset for semantic segmentation of ALS scenes into 7 semantic classes: other, ground, vegetation, building, water, bridge, and permanent structure. This reduced nomenclature is adapted from the Lidar HD nomenclature, which has 11 classes (described in Appendix A). Low, medium, and high vegetation are grouped together since they only differ in height above ground, artefact and synthetic points are simply filtered out, and the “Unclassified” ASPRS class is renamed “other” for clarity. This correspondence between the two nomenclatures is summarized in Figure IV.

We adopt the evaluation practices of similar Lidar datasets (e.g. [12]) and use the mean IoU (mIoU) as our main metric. Importantly, we decide not to exclude class other from metric computations. This class is semantically ill-defined and may include points with blurred boundaries with adjacent classes such as building, ground, and vegetation. However, it also includes well-defined objects such as vehicles and containers. Such objects present a known challenge to segmentation methods, and we believe it is important to account for them in model evaluation.

For consistency with other benchmarks, we also report Overall Accuracy (OA), and precision, recall, and F1 score (for each class and macro-averaged). All metrics should be computed from the accumulated point confusion matrix over all point clouds from the test set, which we also report as part of our baseline evaluation.

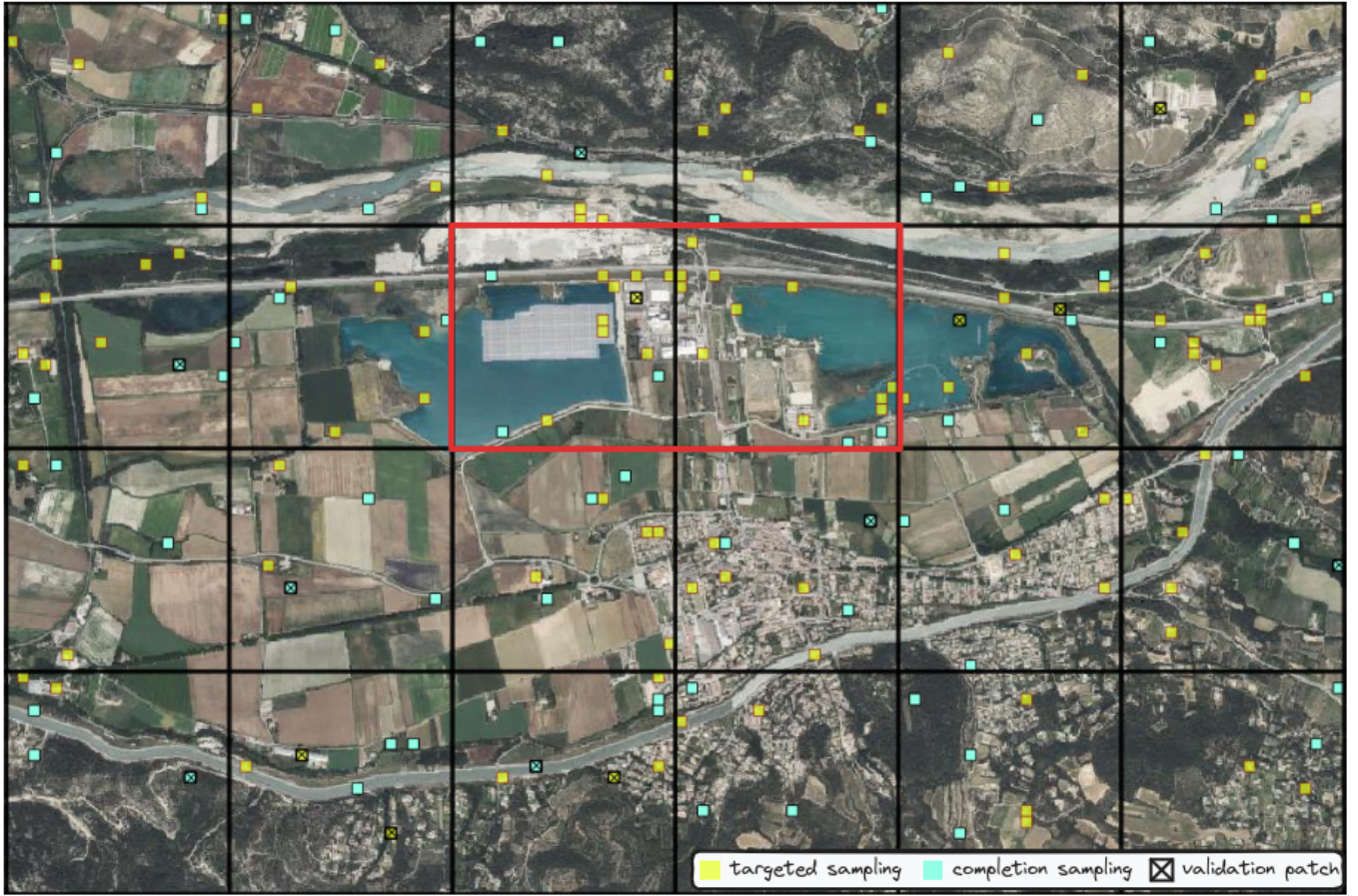


Fig. 5: Patches in FRCTAL on a subset area of 4×6 Lidar HD tiles. Patches selected via targeted sampling (yellow) are more present in complex urban areas. Patches from completion (cyan) sampling are homogeneously distributed.

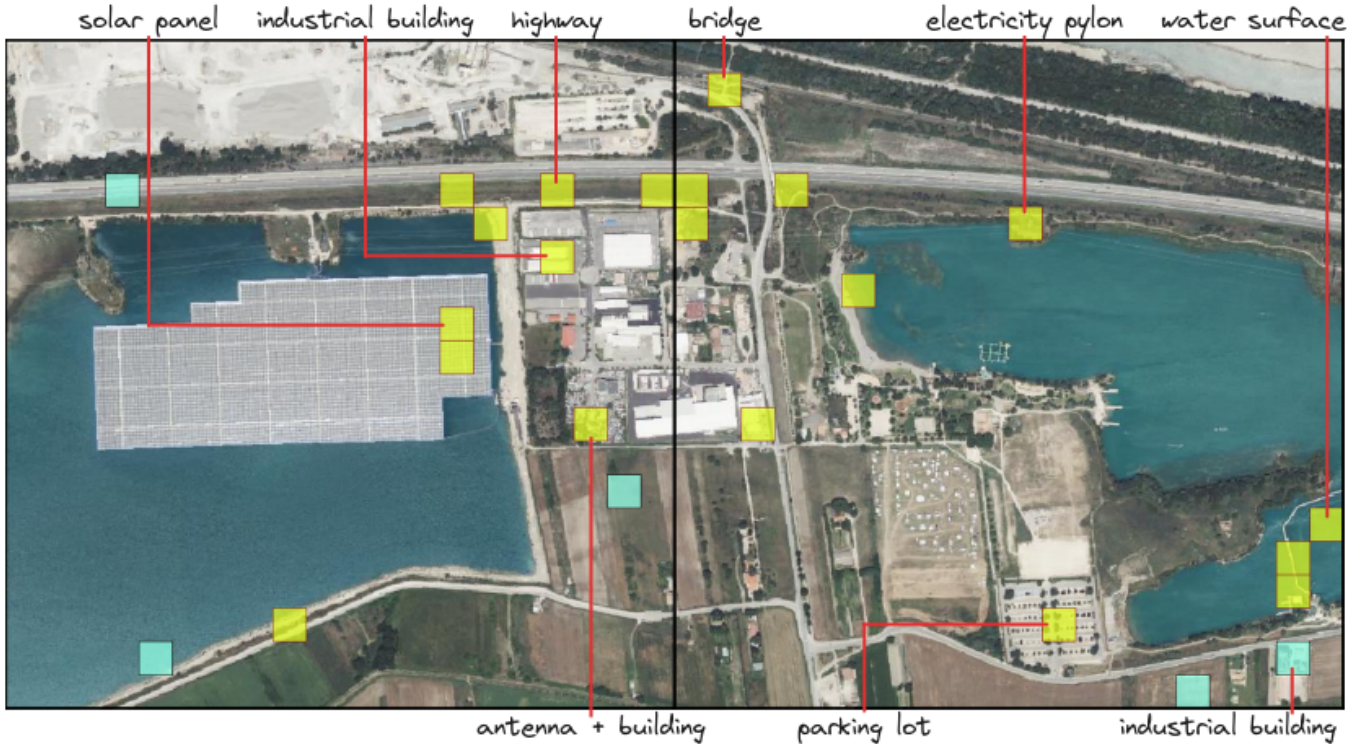


Fig. 6: Enlarged view of 2 Lidar HD tiles showing the difference between targeted sampling and completion sampling. 25 patches are selected from the 800 possible patches, most of which contain scenes of particular interest.

B. Baseline model

The baseline performance is established using Myria3D [24], a 3D deep learning library developed at IGN. Myria3D leverages the Pytorch-Lightning framework [25], and Pytorch-Geometric [26], a powerful library for 3D deep learning.

1) Neural architecture

Myria3D was explicitly built for the semantic segmentation of Lidar HD data, and scalability informed its design, including the choice of its neural architecture: RandLa-Net [27]. Since the PointNet++ architecture [10] succeeded to the ground-breaking PointNet [9] to operate directly on unordered point clouds, there were many attempts to improve over point-based architectures, characterized by PointNet-like operations hierarchically organized in a U-shaped architecture. Conceptually simple, RandLa-Net makes some interesting additions to PointNet++. It uses a lightweight module for local spatial encoding and achieves performance gains thanks to random sampling. Importantly, authors demonstrated its performance in large-scale outdoor Lidar benchmark datasets like SemanticKITTI [28] and Semantic 3D [29].

2) Data processing and training hyperparameters

In our experiments, we kept most defaults setting from Myria3D, which were described in extenso in a previous work. We thus refer the reader to Section *Benchmark Models* in [11] for details on the processing of colorized Lidar HD tiles as well as training hyperparameters (optimizer, learning rate, scheduler, early stopping, etc.).

3) Infrastructure

Training is conducted with 6 NVIDIA Tesla V100 GPUs, each equipped with 32 GB of memory, using Pytorch-Lightning’s distributed data parallel (ddp) strategy. We log all metrics using Comet, a machine learning experiment tracking tool [30]. With this configuration the approximate learning time is 30 minutes per epoch.

C. Experimental results

We report the results obtained using the 80,000 patches for training and 10,000 patches for validation, and testing on the remaining 10,000 patches of the dataset.

1) Quantitative results

The baseline achieves a test mIoU of 77.5% and a test OA of 96.1%. Figure 7 details the IoU results per class. We observe highly accurate results for the three most common classes: ground, vegetation, and building have an IoU above 90%, with a maximum of 93.8% for vegetation. Similarly, class water has an IoU of 90.1%, despite its extreme initial rarity (0.6%) in the sampling area. For classes bridge and permanent structure, also initially rare (0.01% each), the model achieves decent performance with an IoU above 60%. Compared to the six other classes, the baseline underperforms for class other, but still achieves an IoU of 47.5%, which is remarkable considering the fuzzy definition of this class. Based on our own experience with Lidar HD semantic segmentation, these performances can

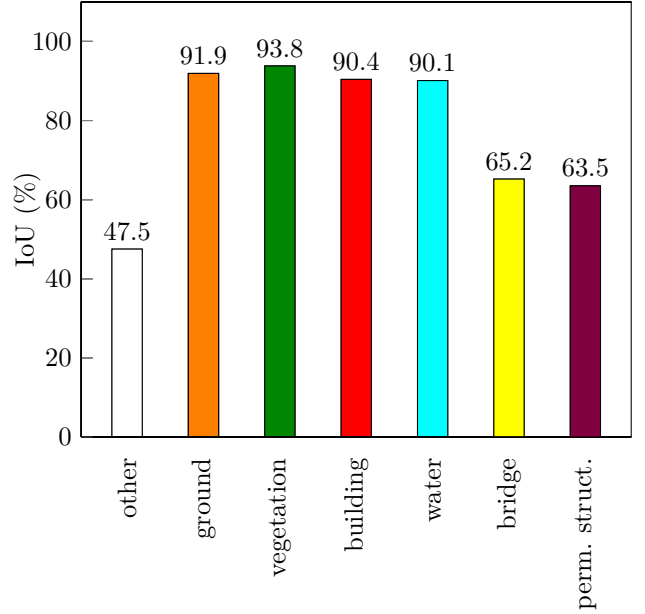


Fig. 7: Baseline per-class test IoUs.

not be achieved without the class rebalancing that happens in the sampling of FRACTAL. For an in-depth performance assessment, all metrics (IoU, precision, recall and F1 score) are reported in Appendix E.

Figure 8 shows the baseline confusion matrix on the test set, normalized by both rows (a) and columns (b). Vegetation, ground, and building have low relative confusion, as expected from their high IoU. Permanent structure has its highest confusion with vegetation, due to the vertical nature and intricate geometries shared by both classes e.g., between pylons and trees. High interclass confusion is also found between classes that may have imprecise geometric boundaries. For example, bridge points are misclassified as ground, of which they are often an extension. Points of class other have high confusion with vegetation and ground points. This is mainly due to the Lidar HD classification specification, which favors specificity over recall for the ground and vegetation classes. As a result, the model may be penalized for accurately identifying ground and vegetation whose target class is other. Note that with only 0.6% of all points in FRACTAL, class other is a small minority, and these errors have a negligible effect on the measured performance for the ground and vegetation classes.

2) Qualitative results

Finally, Figure 9 presents sample predictions of the baseline model for five types of Lidar scenes: a) OTHER_PARKING, b) WATER and BRIDGE, c) URBAN, d) BUILD_GREENHOUSE, and e) HIGHSLOPE1. The 5 patches are selected at random based solely on their scene descriptors, among test patches with at least 10k points (i.e. at least 4 pts/m²). We present the inference results without cherry-picking.

(a) Row-normalized (recall)

Actual	other	54.88	13.02	21.53	9.13	0.42	0.38	0.61
	ground	0.03	97.73	2.07	0.04	0.07	0.03	0
	vegetation	0.1	4.22	95.59	0.07	0	0	0
	building	0.89	3.31	1.6	93.69	0	0.47	0.01
	water	0	7.29	0.06	0	92.63	0	0
	bridge	2.05	15.29	1.25	2.76	0	78.63	0
	permanent structure	8.96	0.79	9.87	2.94	0.04	0.8	76.56
		other	ground	vegetation	building	water	bridge	permanent structure
		Predicted						

(a) Column-normalized (precision)

Actual	other	77.83	0.2	0.27	1.87	0.24	1.62	14.13
	ground	2.78	93.84	1.59	0.51	2.55	8.6	1.27
	vegetation	11.75	5.41	98.01	1.2	0.1	0.19	3.51
	building	6.34	0.26	0.1	96.24	0	10.12	2.18
	water	0.01	0.2	0	0	97.08	0	0
	bridge	0.69	0.05	0	0.13	0	79.28	0.01
	permanent structure	0.56	0	0	0.02	0	0.15	78.87
		other	ground	vegetation	building	water	bridge	permanent structure
		Predicted						

Fig. 8: Baseline test confusion matrices normalized by rows (a) and columns (b). Diagonal values in row-normalized matrix correspond to recall. Diagonal values in column-normalized matrix correspond to precision.

VI. CONCLUSION

We present FRACTAL, an ultra-large-scale benchmark dataset for the 3D semantic segmentation of ALS point clouds. The dataset is based on high quality open data from the French Lidar HD nationwide acquisition program. It is a distillation of a larger initial area of 17,440 km² in five French regions. We show that a simple targeted sampling with spatial stratification at all levels effectively preserves the spatial and semantic diversity of regional-scale volumes of Lidar data. FRACTAL’s size is compatible with deep learning research practices, and it is the largest Lidar benchmark dataset to date, with 9261 million points in 100,000 point clouds and a total span of 250 km². While other ALS benchmark datasets typically cover a single urban area, the large diversity of urban and rural landscapes in FRACTAL is representative of the challenges of 3D semantic segmentation for land monitoring. Thanks to class rebalancing, our methodology opens the possibility of robust assessment of semantic segmentation performance, even for initially rare classes water, bridge, and permanent structure. The baseline evaluation of a 3D neural network (RandLa-Net) further demonstrates the quality of the dataset for model benchmarking. We invite the research community to benchmark both state-of-the-art and novel methods against this dataset. We hope that FRACTAL will advance the field of deep learning for airborne Lidar and ultimately benefit public Lidar-based 3D mapping programs for land monitoring.

CODE AND DATA ACCESS

The dataset is made available on the HuggingFace platform as [IGNF/FRACTAL](#). The sampling, extraction, and colorization of point clouds were conducted with the Patch Catalog Sampling (PaCaSam) code repository available at: [github.com/IGNF/pacasam](#). The baseline model was trained with the Myria3D code repository available at [github.com/IGNF/myria3d](#). Its weights are made available on HuggingFace as [IGNF/FRACTAL-LidarHD_7cl_randlanet](#).

All assets are released under permissive open licences.

ACKNOWLEDGEMENTS

The authors thank Léa Vauchier for her code reviews of the data engineering code, and Marouane Zellou for maintaining the in-house high-performance computing server, and Matthieu Porte and Anatol Garioud for reviewing this data paper. The authors also thank Anatol Garioud for paving the way for the open release of deep learning datasets for land monitoring at IGN with the FLAIR dataset [31].

AUTHORS’ CONTRIBUTION

C.G. established the sampling framework. C.G. and F.R. defined the data descriptors and their target proportions. C.G. implemented the tools for patch sampling and data extraction. F.R. and M.D. defined the specifications for the Lidar Patch Catalog, and M.D. implemented it. C.G. implemented and evaluated the deep learning baseline. C.G. wrote the data paper and released the dataset.

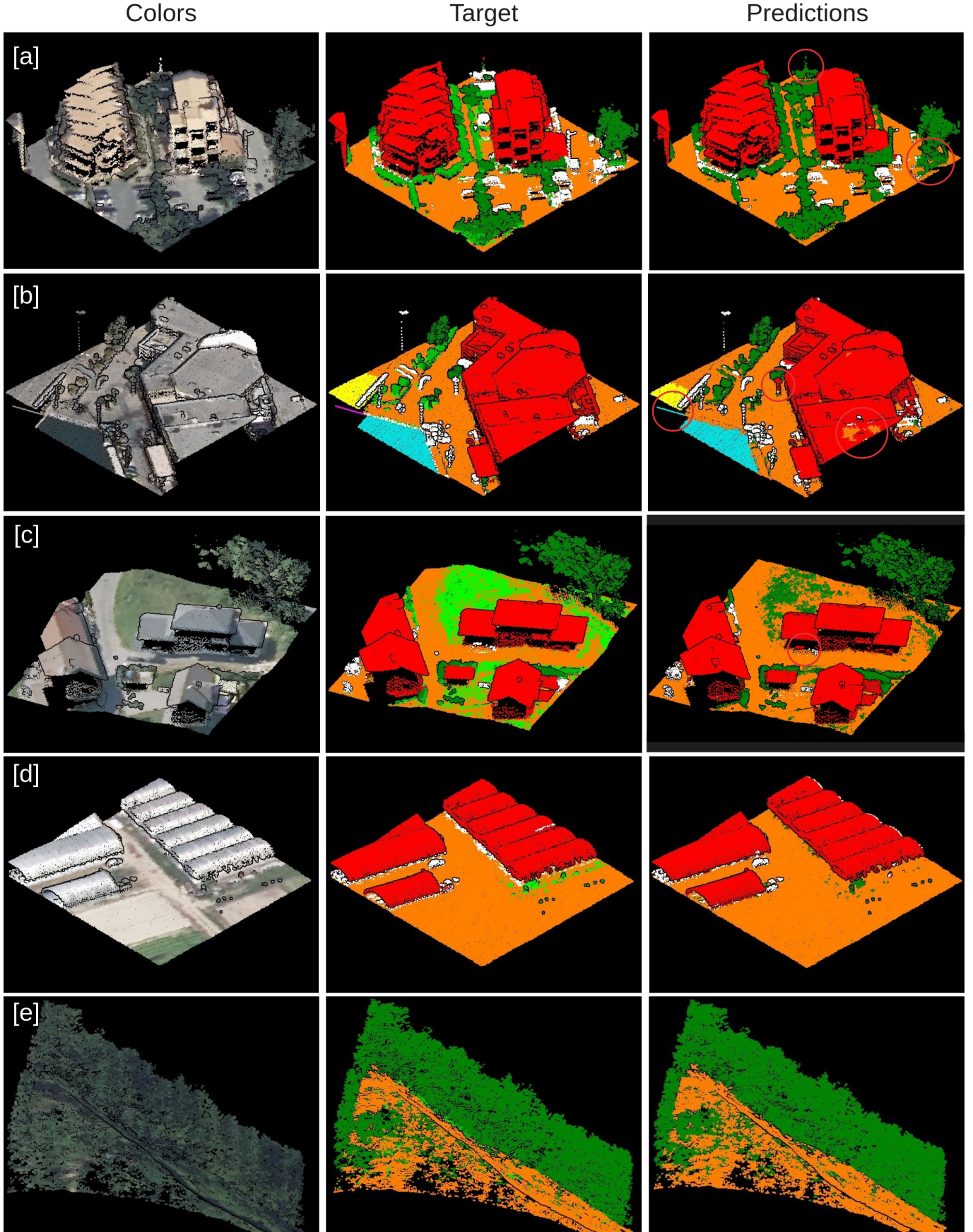


Fig. 9: Input point cloud, target classification, and predictions of the baseline model for a subset of test patches. Patches are selected at random and without cherry-picking, to match the following scene types: a) OTHER_PARKING, b) WATER and BRIDGE, c) URBAN, d) BUILD_GREENHOUSE, and e) HIGHSLOPE1. Color scheme is: other (white), ground (orange), vegetation (green), building (red), water (cyan), bridge (yellow), permanent structure (purple). Predictions errors are circled in red.

REFERENCES

- [1] M. Melin, A. C. Shapiro, and P. Glover-Kapfer, "LiDAR for ecology and conservation - WWF conservation technology series (3)," pp. 24–25, 2017. [Online]. Available: www.researchgate.net/publication/320347018 (pp. 1)
- [2] N. A. Muhadi, A. F. Abdullah, S. K. Bejo, M. R. Mahadi, and A. Mijic, "The use of LiDAR-derived DEM in flood applications: A review," 7 2020. [Online]. Available: www.mdpi.com/2072-4292/12/14/2308 (pp. 1)
- [3] M. Yebra, S. Marselis, A. van Dijk, G. Cary, and Y. Chen, "Using Lidar for forest and fuel structure mapping: Options, benefits, requirements and costs," 2015. [Online]. Available: www.bnhcrc.com.au/sites/default/files/managed/downloads/using_lidar_for_forest_and_fuel_structure_mapping_final.pdf (pp. 1)
- [4] G. Kakoulaki, A. Martinez, and F. Petro, "Non-commercial Light Detection and Ranging (LiDAR) data in Europe," 2021. [Online]. Available: <https://doi.org/10.2760/212427> (pp. 1)
- [5] Institut national de l'information géographique et forestière (IGN), "Lidar HD [Database]," 1 2023. [Online]. Available: www.geoservices.ign.fr/documentation/donnees/alti/lidarhd (pp. 1, 2, 3)
- [6] "TopoDOT [software]." [Online]. Available: www.topodot.com (pp. 1)
- [7] "TerraScan [software]." [Online]. Available: terrasolid.com/products/terrascan (pp. 1)
- [8] K. Yen, "Automated LiDAR extraction software," 2021. [Online]. Available: <https://dot.ca.gov/-/media/dot-media/programs/research-innovation-system-information/documents/preliminary-investigations/pi-0324-lidarsoftwarepi.pdf> (pp. 1)
- [9] C. R. Qi, H. Su, K. Mo, and L. J. Guibas, "PointNet: Deep learning on point sets for 3D classification and segmentation," *Arxiv*, 12 2016. [Online]. Available: <https://arxiv.org/abs/1612.00593> (pp. 1, 9)
- [10] C. R. Qi, L. Yi, H. Su, and L. J. Guibas, "PointNet++: Deep hierarchical feature learning on point sets in a metric space," *Arxiv*, 6 2017. [Online]. Available: <https://arxiv.org/abs/1706.02413> (pp. 1, 9)
- [11] C. Gaydon and F. Roche, "PureForest: A large-scale aerial lidar and aerial imagery dataset for tree species classification in monospecific forests," 4 2024. [Online]. Available: <https://arxiv.org/abs/2404.12064> (pp. 1, 9)
- [12] N. Varney, V. K. Asari, and Q. Graehling, "DALES: A large-scale aerial LiDAR data set for semantic segmentation," *ArXiv*, 4 2020. [Online]. Available: <http://arxiv.org/abs/2004.11985> (pp. 1, 2, 7)
- [13] P. Zachar, K. Bakula, and W. Ostrowski, "CENAGIS-ALS Benchmark - new proposal for dense ALS benchmark based on the review of datasets and benchmarks for 3D point cloud segmentation," vol. 48. International Society for Photogrammetry and Remote Sensing, 10 2023, pp. 227–234. [Online]. Available: <https://doi.org/10.5194/isprs-archives-XLVIII-1-W3-2023-227-2023> (pp. 2, 2, 2)
- [14] N. Qin, W. Tan, L. Ma, D. Zhang, and J. Li, "OpenGF: An ultra-large-scale ground filtering dataset built upon open ALS point clouds around the world." [Online]. Available: <https://arxiv.org/abs/2101.09641> (pp. 2, 2)
- [15] J. Niemeyer, F. Rottensteiner, and U. Soergel, "Contextual classification of lidar data and building object detection in urban areas," *ISPRS Journal of Photogrammetry and Remote Sensing*, vol. 87, pp. 152–165, 1 2014. [Online]. Available: <https://doi.org/10.1016/j.isprsjprs.2013.11.001> (pp. 2)
- [16] S. M. I. Zolanvari, S. Ruano, A. Rana, A. Cummins, R. E. da Silva, M. Rahbar, and A. Smolic, "DublinCity: Annotated LiDAR point cloud and its applications," 9 2019. [Online]. Available: <http://arxiv.org/abs/1909.03613> (pp. 2)
- [17] Z. Ye, Y. Xu, R. Huang, X. Tong, X. Li, X. Liu, K. Luan, L. Hoegner, and U. Stilla, "LASDU: A large-scale aerial LiDAR dataset for semantic labeling in dense urban areas," *ISPRS International Journal of Geo-Information*, vol. 9, 7 2020. [Online]. Available: <https://doi.org/10.3390/ijgi9070450> (pp. 2)
- [18] M. Kölle, D. Laupheimer, S. Schmohl, N. Haala, F. Rottensteiner, J. D. Wegner, and H. Ledoux, "The Hessigheim 3D (H3D) benchmark on semantic segmentation of high-resolution 3D point clouds and textured meshes from UAV LiDAR and Multi-View-Stereo," *ISPRS Open Journal of Photogrammetry and Remote Sensing*, vol. 1, p. 100001, 10 2021. [Online]. Available: <https://doi.org/10.1016/j.ophoto.2021.100001> (pp. 2)
- [19] Institut national de l'information géographique et forestière (IGN), "LiDAR HD version 1.0 - descriptif de contenu des nuages de points LiDAR," 10 2023. [Online]. Available: www.geoservices.ign.fr/sites/default/files/2023-10/DC_LiDAR_HD_1-0_PTS.pdf (pp. 3, 5, 13)
- [20] —, "ORTHO HR [Database]," 1 2023. [Online]. Available: www.geoservices.ign.fr/bdortho (pp. 3)
- [21] T. Kattenborn, F. Schiefer, J. Frey, H. Feilhauer, M. D. Mahecha, and C. F. Dormann, "Spatially autocorrelated training and validation samples inflate performance assessment of convolutional neural networks," *ISPRS Open Journal of Photogrammetry and Remote Sensing*, vol. 5, 8 2022. [Online]. Available: <https://doi.org/10.1016/j.ophoto.2022.100018> (pp. 3)
- [22] Institut national de l'information géographique et forestière (IGN), "Bd topo® [database]," 2024. [Online]. Available: www.geoservices.ign.fr/bdtopo (pp. 4)
- [23] The American Society for Photogrammetry and Remote Sensing, "LAS specification 1.4 - R15," 2019. [Online]. Available: www.asprs.org/wp-content/uploads/2019/07/LAS_1_4_r15.pdf (pp. 5)
- [24] C. Gaydon, "Myria3D: Deep learning for the semantic segmentation of aerial Lidar point clouds [software]," 2022. [Online]. Available: www.github.com/IGNF/myria3d (pp. 9)
- [25] W. Falcon and T. P. L. team, "PyTorch Lightning [software]," 3 2019. [Online]. Available: www.github.com/Lightning-AI/lightning (pp. 9)
- [26] M. Fey and J. E. Lenssen, "Fast graph representation learning with PyTorch Geometric," 2019. [Online]. Available: www.github.com/pyg-team/pytorch_geometric (pp. 9)
- [27] Q. Hu, B. Yang, L. Xie, S. Rosa, Y. Guo, Z. Wang, N. Trigoni, and A. Markham, "RandLA-Net: Efficient semantic segmentation of large-scale point clouds," *Arxiv*, 11 2019. [Online]. Available: <https://arxiv.org/abs/1911.11236> (pp. 9)
- [28] J. Behley, M. Garbade, A. Milioto, J. Quenzel, S. Behnke, C. Stachniss, and J. Gall, "SemanticKITTI: A dataset for semantic scene understanding of LiDAR sequences," 2019. [Online]. Available: <https://arxiv.org/abs/1904.01416> (pp. 9)
- [29] T. Hackel, N. Savinov, L. Ladicky, J. D. Wegner, K. Schindler, and M. Pollefeys, "SEMANTIC3D.NET: A new large-scale point cloud classification benchmark," vol. IV-1-W1, 2017, pp. 91–98. [Online]. Available: <http://www.semantic3d.net> (pp. 9)
- [30] Comet ML, "Comet [ML platform]," 2024. [Online]. Available: www.comet.com (pp. 9)
- [31] A. Garioud, N. Gonthier, L. Landrieu, A. D. Wit, M. Valette, M. Poupée, S. Giordano, and B. Wattrélos, "FLAIR: a country-scale land cover semantic segmentation dataset from multi-source optical imagery," 2023. [Online]. Available: <https://doi.org/10.48550/arXiv.2310.13336> (pp. 10)

A Specifications of the Lidar HD classification.

RGB	Value	Name	Content
255,255,255	1	Unclassified	All points that do not belong in any of the other classes. For example, it includes vehicles, animals or people, temporary objects, wood piles, etc.
255,128,0	2	Ground	Points located on the surface of natural and artificial ground. Bridge decks are not part of this class.
0,255,0	3	Low vegetation	Trees, shrubs and low vegetation (e.g. bushes, ferns, reeds, etc.). Vegetation at ground level (less than 20 cm high, typically grass) is classified as vegetation only if there are enough ground points locally for ground modeling. The class also includes cultivated trees (orchards, vineyards, field crops, etc.). Vegetation is further divided into 3 classes based on height above ground: low ($< 0.5\text{m}$), medium (between 0.5 m and 1.5 m), and high ($\geq 1.5\text{ m}$) vegetation.
0,193,0	4	Medium vegetation	
0,134,0	5	High vegetation	
255,0,0	6	Building	A building is defined as a permanent structure with an area greater than 10 m ² . Besides residential buildings it includes monuments, castles, mills, water towers, lighthouses, industrial chimneys, ramparts and fortifications. The specification also includes roofs and façades, as well as chimneys, dormer windows, skylights and balconies. As the permanent nature of a structure cannot be established from lidar data only, this class may include lightweight structures without walls such as garden sheds, bungalows, market canvases or awnings.
0,225,225	9	Water	All points located on the surface of rivers, bodies of water, sea, or ocean.
255,255,0	17	Bridge deck	A bridge is an engineering structure passing over one or more elements of the road, rail or waterway network. Point on bridge decks are included, while structural elements such as piers and parapets are assigned to the "Unclassified" class. Very high structural elements ($\geq 5\text{ m}$ above deck level) such as piers and abutments are classified as "Permanent structures". Tunneled passages (including nozzles, which are openings in the ground generally to allow water to drain) are considered part of the ground and therefore excluded.
128,0,64	64	Permanent structures	All aboveground objects other than buildings, vegetation and bridges, that are identified as perennial and of such a nature that they characterize the landscape. This class includes (but is not limited to): wind turbines, cable cars, telecommunication antennas, electricity distribution networks (cables and pylons), bridge elements above the deck (cables, piers, etc.).
64,0,128	65	Artefact	All points that do not correspond to an actual object or terrain.
255,0,255	66	Synthetic	Artificial points created under bridges and and on water surfaces to have coherent digital models.

Refer to the Lidar HD product description [19] for more specifications.

B Sensors used to acquire Lidar HD data in each of the 8 50×50 km blocks represented in FRACTAL.

Block	Sensor	Subcontractor(s)	
		Acquisition	Classification
GN	CityMapper 2H: Hyperion 2+	APEI + Avineon	Avineon
MQ	RIEGL VQ1560 II-S	Eurosense + SFS	Eurosense + SFS
MP	RIEGL VQ-1560 II	Eurosense	Sintégra
PK	RIEGL VQ1560 II	Eurosense	Eurosense
PO	Leica CityMapper-2	Avineon + APEI	Avineon + APEI
PP	Leica CityMapper-2	Avineon + APEI	Eurosense + SFS
QO	RIEGL VQ780 II-S	Sintégra + Bluesky	Sintégra + Bluesky
UT	RIEGL VQ780 II-S	Sintégra + Bluesky	Avineon + APEI

N.B. Data acquisition and its classification were often conducted by distinct subcontractors, which we also report.

C Number of points by class in the sampling area, in the dataset, and in the train, val and test sets.

Name	FRACTAL									
	Sampling Area		FRACTAL		Train		Val		Test	
	Points (M)	%	Points (M)	%	Points (M)	%	Points (M)	%	Points (M)	%
Other	2,137	0.32	53	0.57	41	0.56	5	0.53	6	0.66
Ground	258,751	39.1	3,625	39.1	2,874	39.0	359	39.1	391	40.5
Vegetation	394,425	59.6	5,248	56.7	4,203	57.0	523	56.9	523	54.1
Building	4,939	0.75	264	2.85	206	2.80	26	2.80	32	3.33
Water	1,504	0.23	54	0.59	38	0.52	5	0.49	12	1.20
Bridge	47	0.01	12	0.13	9	0.13	1	0.10	2	0.16
Permanent structure	33	0.01	3	0.04	3	0.04	0	0.04	0	0.03
Total	661998	-	9261	-	7376	-	919	-	966	-

D Proportions of scene types in the train, val, and test sets.

Descriptor	Train (%)	Val (%)	Test (%)
BUILD	22.5	22.8	25.7
BUILD_BIG	5	4.8	4.9
BUILD_GREENHOUSE	1.3	1.3	1.2
BRIDGE	5.5	5.4	5.4
WATER	8.2	8.1	11
WATER_SURFACE	6	5.9	7.7
PERMSTRUCT	5	4.9	4.6
PERMSTRUCT_ANTENNA	0.9	0.9	0.6
PERMSTRUCT_PYLON	1.5	1.4	1.4
OTHER	22.7	22.6	27.5
OTHER_HIGHWAY	1.3	1.2	1.7
OTHER_PARKING	1.1	1.1	1.5
FOREST	7.3	7.4	7.1
HIGHSLOPE1	11.5	11.8	11
HIGHSLOPE2	5.5	5.4	4.8
MOUTAIN	17.4	17.6	14.5
WATER_ONLY	1.7	1.7	4.5
SEASHORE	1.4	1.4	4.5
URBAN	6.4	6.5	7.4

E Baseline test IoU, precision, recall and F1 score for each semantic class and macro-averaged.

Class	IoU	Accuracy	Precision	Recall	F1 Score
other	47.5	54.9	77.8	54.9	64.4
ground	91.9	97.7	93.8	97.7	95.8
vegetation	93.8	95.6	98.0	95.6	96.8
building	90.4	93.7	96.2	93.7	95.0
water	90.1	92.6	97.1	92.6	94.8
bridge	65.2	96.1	79.3	78.6	79.0
permanent structure	63.5	76.6	78.9	76.6	77.7
Macro Average	77.5	86.7	88.7	84.2	86.2